Human Microsomal Prostaglandin E Synthase-1 (mPGES-1) Binding with Inhibitors and the Quantitative Structure−Activity Correlation

Mohamed Diwan M. AbdulHameed, Adel Hamza, Junjun Liu, Xiaoqin Huang, and Chang-Guo Zhan*

Department of Pharmaceutical Sciences, College of Pharmacy, University of Kentucky, 725 Rose Street, Lexington, Kentucky 40536

Received August 21, 2007

The detailed structures of microsomal prostaglandin E synthase-1 (mPGES-1) binding with inhibitors have been studied, for the first time, by using a newly developed computational three-dimensional (3D) structural model of mPGES-1 along with a 3D-quantitative structure−activity relationship (3D-QSAR) analysis. The obtained satisfactory binding structures and 3D-QSAR models strongly suggest that the 3D structural model of mPGES-1 is reasonable for study of mPGES-1 binding with inhibitors and for future design of novel mPGES-1 inhibitors.

INTRODUCTION

Microsomal prostaglandin E synthase-1 (mPGES-1) is the terminal enzyme in the prostaglandin (PG) biosynthesis pathway and catalyzes the conversion of prostaglandin H_2 (PGH_2) to prostaglandin E_2 (PGE_2).[1] It is an inducible enzyme, and its expression is increased in response to proinflammatory stimuli.[2,3] Studies on mPGES-1 have established its role in a number of disease conditions including inflammation, arthritis, fever, pain, cancer, stroke, and bone disorders.[4−10] PGE_2 produced by mPGES-1 is a well-characterized mediator of inflammation and pain.[11] The known nonsteroidal anti-inflammatory drugs (NSAIDS) target PG pathway and inhibit either cyclooxygenase (COX)-1 or COX-2.[12] But the COX inhibitors have shown many side effects including ulcers and cardiovascular diseases.[13−15] Grosser et al. have shown that the biological basis for the cardiovascular side effects of COX-2 inhibitors is target specific.[16] By inhibiting COX-2, the functions of all downstream PG synthases are blocked, including prostacyclin synthase (PGIS) for the conversion of PGH_2 to prostacyclin I_2 (PGI_2). Blocking the production of PGI_2 has been reported to play a role in cardiovascular side effects.[17] In this situation, inhibition of the downstream enzyme mPGES-1 has emerged as a novel strategy which will target only the PGE_2 pathway and without any adverse effects expected in the COX-2 inhibition.[18] Thus mPGES-1 has emerged as a more attractive target for design and discovery of the next-generation therapeutics, especially for the treatment of inflammation-related diseases.

Very few inhibitors of mPGES-1 were identified in experimental screening efforts. Riendeau et al.[19] have recently reported a series of mPGES-1 inhibitors (see below) synthesized based on the scaffold of MK-886 (an anticancer drug which can more potently bind with at least one other protein). Some of these newly synthesized mPGES-1 inhibitors are potent, with an IC_{50} value of a few nM in vitro. However, none of these inhibitors is specific for mPGES-1 such that all of these compounds have a very low activity against mPGES-1 in vivo. It is highly desirable to design and discover novel, mPGES-1-specific inhibitors with different scaffolds.

One of the major impeding factors for rational design and discovery of novel mPGES-1 inhibitors is the absence of a detailed three-dimensional (3D) X-ray crystal structure of mPGES-1, as it is generally difficult to produce a qualified single crystal for a membrane protein such as mPGES-1. We recently reported for the first time a 3D structural model of the substrate-binding domain (SBD) of mPGES-1.[20] This 3D model was constructed by developing and using an ab initio approach of the protein structure prediction. The 3D model was also used to explore how mPGES-1 binds with its substrates PGH_2 and glutathione (GSH). The predicted enzyme−substrate binding mode was examined by performing site-directed mutagenesis and the enzyme activity tests on various mPGES-1 mutants. The data obtained from the wet experimental tests are qualitatively consistent with the 3D model of mPGES-1, suggesting that the 3D model is reasonable. How good is the 3D model of mPGES-1 for studying the enzyme−inhibitor binding? The 3D structural model of mPGES-1 provides a unique opportunity for us, in the present study, to further explore how mPGES-1 binds with inhibitors and to predict the modes of the enzyme−inhibitor binding by carrying out molecular docking. Molecular docking is a popularly used computational approach in understanding protein−ligand binding and structure-based drug design.[21]

Further, as a computational 3D structural model of mPGES-1 is usually not as reliable as an X-ray crystal structure, we were also interested in exploring the enzyme−inhibitor binding modes by using a different computational strategy which does not rely on the 3D structural model of mPGES-1 in order to know whether two completely different computational strategies lead to the consistent insights concerning the enzyme−inhibitor binding. Hence, we also performed a detailed 3D-quantitative structure−activity relationship (3D-QSAR) analysis on the known mPGES-1

* Corresponding author e-mail: zhan@uky.edu.

10.1021/ci700315c CCC: $40.75
Published on Web 12/04/2007

Table 1. Molecular Structures of the Compounds Used in the Training Set and the Test Set and Their mPGES-1 Inhibitory Activity[a]

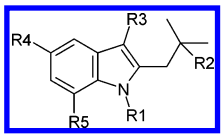

compd	R1	R2	R3	R4	R5	IC_{50} (μM)
			Training Set			
1	CH_2(4-Cl−Ph)	COO^-	S-^{t}Bu	^{i}Pr	H	1.6
2	H	COO^-	S-^{t}Bu	^{i}Pr	H	>10
3	Me	COO^-	S-^{t}Bu	^{i}Pr	H	>10
4	CH_2(CH═CH_2)	COO^-	S-^{t}Bu	^{i}Pr	H	6.7
5	$(CH_2)_3$Ph	COO^-	S-^{t}Bu	^{i}Pr	H	3.2
8	CH_2(4-Cl−Ph)	COO^-	Ph	^{i}Pr	H	6.4
9	CH_2(4-Cl−Ph)	COO^-	OPh	^{i}Pr	H	0.65
10	CH_2(4-Cl−Ph)	COO^-	CH_2(4-^{t}Bu−Ph)	^{i}Pr	H	0.29
11	CH_2(4-Cl−Ph)	COO^-	CO(2-Me−Ph)	^{i}Pr	H	0.90
12	CH_2(4-Cl−Ph)	COO^-	COCH2S-^{t}Bu	^{i}Pr	H	0.26
13	CH_2(4-Cl−Ph)	COO^-	COCH2-^{t}Bu	^{i}Pr	H	0.25
15	CH_2(4-Cl−Ph)	COO^-	Me	H	^{i}Pr	4.3
16	CH_2(4-Cl−Ph)	COO^-	Me	H	H	3.2
17	CH_2(4-Cl−Ph)	COO^-	Me	F	H	2.6
18	CH_2(4-Cl−Ph)	COO^-	Me	^{t}Bu	H	0.33
20	CH_2(4-Cl−Ph)	COO^-	Me	(3-Ph)-Ph	H	0.16
21	CH_2(4-Cl−Ph)	COO^-	Me	(4-Ph)-Ph	H	0.016
23	CH_2(4-Cl−Ph)	COO^-	Me	(3-F,4-Ph)-Ph	H	0.007
24	CH_2(4-Cl−Ph)	COO^-	Me	(3-F,4-Pyrz)-Ph	H	0.032
25	CH_2(4-Cl−Ph)	COO^-	Me	(3-F,4-Pyr)-Ph	H	0.012
26	CH_2(4-Cl−Ph)	COO^-	Me	[3-F,4-(2-MeO−Ph)]-Ph	H	0.005
28	CH_2(4-Cl−Ph)	COO^-	Me	[3-F,4-(2-F−Ph)]-Ph	H	0.008
29	CH_2(4-Cl−Ph)	COO^-	Me	[3-F,4-(2-MeCO−Ph)]-Ph	H	0.006
30	CH_2(4-Cl−Ph)	COO^-	Me	[3-F,4-(2-Me−Ph)]-Ph	H	0.003
31	CH_2(4-Cl−Ph)	COO^-	Me	[3-F,4-(3-Me−Ph)]-Ph	H	0.033
32	CH_2(4-Cl−Ph)	COO^-	Me	[3-F,4-(4-Me−Ph)]-Ph	H	0.031
			Test Set			
6	CH_2(4-Cl−Ph)	CO_2Me	S-^{t}Bu	^{i}Pr	H	7.2
7	CH_2(4-Cl−Ph)	$CONH_2$	S-^{t}Bu	^{i}Pr	H	>10
14	CH_2(4-Cl−Ph)	COO^-	Me	^{i}Pr	H	1.1
19	CH_2(4-Cl−Ph)	COO^-	Me	Ph	H	0.60
22	CH_2(4-Cl−Ph)	COO^-	Me	(3-Cl,4-Ph)-Ph	H	0.022
27	CH_2(4-Cl−Ph)	COO^-	Me	[3-F,4-(2-Cl−Ph)]-Ph	H	0.004

[a] Ph = phenyl; ^{i}Pr = isopropyl; ^{t}Bu = *tert*-butyl.

inhibitors.[19] The 3D-QSAR analysis without using the 3D structural model of mPGES-1 and the molecular docking using the 3D structural model of mPGES-1 can be used as two independent approaches that can complement each other in exploring the enzyme−inhibitor binding modes. Hence, both the 3D-QSAR analysis and molecular docking were carried out, in the present study, to understand how mPGES-1 binds with its inhibitors. At the time of initial submission of this manuscript for consideration of publication, we noticed that a similar 3D-QSAR analysis on the same set of compounds appeared in literature.[22] In comparison with the pure 3D-QSAR analysis, our combined molecular docking and more sophisticated 3D-QSAR analysis provide more detailed structural insights into the enzyme−inhibitor binding. The structural insights obtained from our 3D-QSAR analysis are all consistent with the binding modes determined by the molecular docking, thus further demonstrating that the 3D structural model of mPGES-1 and the binding structures determined are reasonable. The determined binding structures are expected to provide a good starting point for carrying out virtual screening and new lead identification in future drug design and discovery efforts.

COMPUTATIONAL METHODS

Two 3D-QSAR methods were used in this study, i.e., comparative molecular field analysis (CoMFA) and comparative molecular similarity indices analysis (CoMSIA) implemented in SYBYL software.[23] In CoMFA, the biological activity of molecules is correlated with their steric and electrostatic energies.[24] The steric and electrostatic interaction energies are calculated using Lennard-Jones potential and Coulombic potential, respectively. In CoMSIA, similarity indices are calculated at regularly placed grid points for the aligned molecules. CoMSIA includes additional molecular descriptors like hydrophobic fields and hydrogen bond donor and acceptor fields. Both 3D-QSAR methods give contour maps as an output that can be used to get some general insights into the topological features of the binding site. All compounds used (see Table 1, in which $pIC_{50} = -\log IC_{50}$) to develop the 3D-QSAR models were reported recently by Riendeau et al. as inhibitors of mPGES-1.[19] Of the 32 compounds, 26 compounds were used as a training set and the remaining 6 compounds were used as a test set, based on a random selection. The compounds in the test set have a range of biological activity values similar to that of the

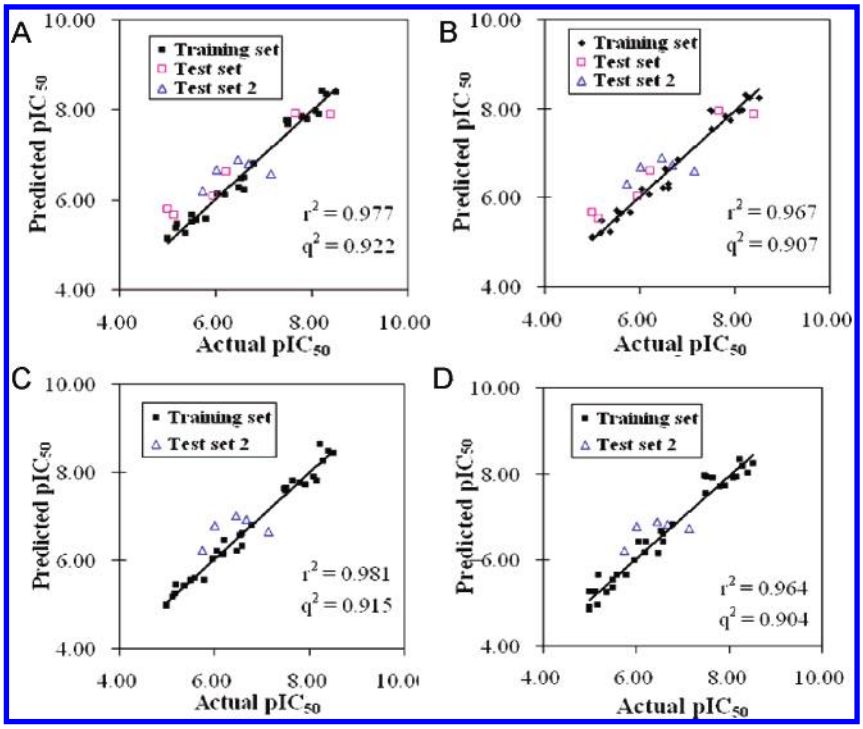

Figure 1. Plots of the predicted pIC_{50} values versus the actual pIC_{50} values. Test set means the external test set of 6 compounds from the series reported by Riendeau et al. (ref 19). Test set 2 refers to the external test set of 5 compounds described in a patent report (ref 27). (A) The CoMFA-1a model using the training set of 26 compounds. (B) The CoMSIA-1b model using the training set of 26 compounds. (C) The CoMFA-2a model using the training set of 32 compounds. (D) The CoMSIA-2b model using the training set of 32 compounds.

training set. A separate model was also developed using all of the 32 compounds as the training set.

Geometries of all compounds used in the 3D-QSAR model development were optimized by using the PM3 semiempirical molecular orbital method. The optimized geometries were used to perform single-point ab initio calculations at the HF/6-31G* level in order to determine the electrostatic potential-fitted atomic charges, i.e., the ESP charges, that fit to the electrostatic potential at points selected according to the Merz−Singh−Kollman scheme implemented in the Gaussion03 program.[25] The carboxyl group in all molecules was assumed to be in the deprotonated state. The most active compound, i.e., **30**, in the series was used as the template for the alignment of all molecules. Molecular docking was carried out by using the FlexX module of SYBYL software.[26] The binding structure was determined by performing a conformational search of the ligand in the active site using the modeled 3D structure of mPGES-1.[20] Only the best conformation was built upon, and the others are discarded. In the previous study, the binding structure of the substrate PGH_2 with mPGES-1 was modeled.[20] Thirty docked orientations were generated for each ligand, and the best docked structure was selected.

RESULTS AND DISCUSSION

3D-QSAR Analysis. To develop the best possible CoMFA and CoMSIA models using the training set of 26 compounds, we tested various alignment rules, combinations of the descriptors, and numbers of principal components (NOP). The 3D-QSAR models were analyzed in terms of a number of statistical parameters, namely the leave-one-out (LOO) cross-validated correlation coefficient (q^2), non-cross-validated correlation coefficient (r^2), standard error estimate (SEE), and F-statistic values. The detailed results of the model tests are provided in the Supporting Information. The best CoMFA model (denoted by CoMFA-1a) has a q^2 value of 0.922, an r^2 value of 0.977, and an SEE value of 0.191. The best CoMSIA model (denoted by CoMSIA-1b) has a q^2 value of 0.907, an r^2 value of 0.967, and an SEE value of 0.229. The high r^2 and q^2 values along with the low SEE values suggest that the models are reasonable and should have a good predictive ability. Compared to the 3D-QSAR study reported by Juan et al.,[22] our use of the more reasonable molecular geometries, atomic charges, and alignment method led to more reasonable 3D-QSAR models (e.g. with higher q^2 and r^2 values). For a remarkable difference between our 3D-QSAR models and those reported by Juan et al.,[22] one compound was found to be an outlier in the CoMFA analysis reported by Juan et al.,[22] whereas our CoMFA and CoMSIA models both are able to reasonably predict the activity for all of the compounds. No outlier was found in our 3D-QSAR models.

The predictive ability of the 3D-QSAR models were further validated using an external test set of 6 compounds. Both CoMFA-1a and CoMSIA-1b gave good predictions for the training and the test set compounds (see Figure 1; the pIC_{50} values are provided in the Supporting Information). In addition, another set of 5 compounds described in a patent report[27] by another group was also used as test set 2 to further examine the predictive ability of the model (see the Supporting Information for the structures of the compounds in test set 2). As seen in Figure 1, the deviations of the predicted pIC_{50} values from the corresponding experimental pIC_{50} values are always significantly smaller than 1 log unit. Our final 3D-QSAR models (i.e., CoMFA-2a and CoMSIA-2b) were developed using all of the 32 compounds as the training set. For the CoMFA-2a model obtained in this way, we have

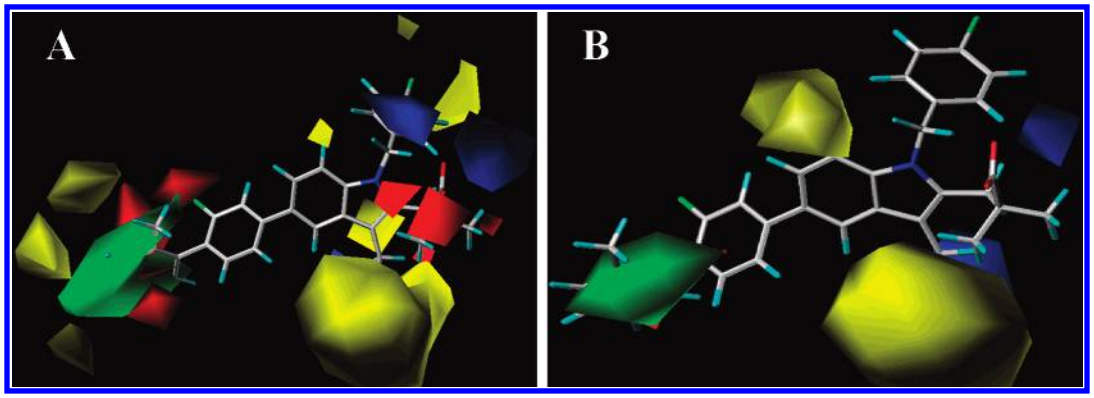

Figure 2. (A) CoMFA steric and electrostatic contour maps around compound **30**. (B) CoMSIA steric and electrostatic contour maps around compound **30**. Green isopleths enclose areas where a steric bulk could enhance the activity. Yellow contours are areas where the steric interaction is disfavored. The blue region represents the area where a positive charge is favorable for the binding. The red region refers to the area where a negative charge is favorable for the binding.

$r^2 = 0.981$, $q^2 = 0.915$, and SEE = 0.176. For the CoMSIA-2b model, we have $r^2 = 0.964$, $q^2 = 0.904$, and SEE = 0.239. Depicted in Figure 1 are plots of the predicted versus the actual pIC_{50} values.

The greatest advantage of the CoMFA and CoMSIA modeling is the visualization of the results as 3D-coefficient contour plots that are extremely useful to gain some valuable information about the ligand-binding site in cases where the target structure is not available. The contour maps were generated as scalar products of coefficients and standard deviation (stdev*coeff), associated with each CoMFA or CoMSIA column. The contour plots (e.g. Figure 2) generated using the final CoMFA-2a and CoMSIA-2b models reveal how the steric and electrostatic factors affect the biological activity of these inhibitors. For example, the most active compound (**30**) in the series is shown superimposed with the CoMFA contour maps in Figure 2(A). The large green contour region surrounding the terminal phenyl ring shows that the steric interaction is favored in this region. This is consistent with the reported experimental results, since compounds **21**−**32** have a terminal phenyl or heteroaryl group in this region and all have the activity with $IC_{50} <$ 100 nM.[19] Further, the favorable steric region is surrounded by an unfavorable yellow region, which shows that more substitutions with bulky groups are not favored. Position #3 of the indole ring is surrounded by a yellow region. This shows that bulky groups are not favored in this region. This explains the lower activity of 3-S-*tert*-butyl substituted compounds like compounds **1**−**7** (IC_{50} = 1.6−10 μM) as well as 3-phenyl substituted compounds (e.g. compound **8**). The bulky substituents at this position are present in the unfavorable yellow region. In the case of compound **10** or **11**, the presence of -CH_2- or a carbonyl group orients the bulky group away from the unfavorable region, and this corresponds to the increased activity of these compounds. This illustrates that the CoMFA model developed can explain the observed differences in the activity of this series of compounds. The yellow contour is also present near position #7 of the indole ring. Compound **15** (IC_{50} = 4.5 μM) has a bulky isopropyl group at position #7, which explains the lower activity of this compound. The yellow contour surrounding the benzyl group at position #1 shows that the further bulky substituent in this group is not favored.

The electrostatic contour plots are shown in blue and red contours. Near the carboxylate group there are red contour regions showing that an electronegative group is favored in these regions. Red contour regions are also present near the terminal phenyl ring. This shows that electronegative groups are favored in the terminal phenyl ring. According to the reported experimental data,[19] the compounds with an electronegative group in the terminal phenyl ring, such as **27**−**29**, show a higher activity. The blue contour region corresponds to the region where an electropositive group is favored. Two blue contours are present close to the benzyl group at position #1 of the indole ring. This contour plots show that the activity can be enhanced by substituting with electropositive substituents in these regions. Similarly, the blue contour near position #3 of the indole ring shows that an electropositive substituent is favored, and electronegative groups are not favored in this region.

Based on the above discussion of the CoMFA contour maps, the terminal phenyl ring is essential for the higher-activity compounds. To increase the inhibitory activity of the compounds, electronegative substituents can be introduced on the terminal phenyl ring. Further introduction of bulky substitution is not favored. Similarly, an appropriate introduction of electropositive groups near the #3 position of the indole ring could also enhance the inhibitory activity.

Binding Structures Obtained from Molecular Docking. Molecular docking using the computationally predicted 3D structural model of mPGES-1 was performed for several purposes in the present study. First of all, we would like to further examine the computationally predicted 3D structural model of mPGES-1 and to know whether the 3D structural model is reasonable or not for studying how mPGES-1 binds with inhibitors. Second, we would like to know the mode of the inhibitors binding with mPGES-1. Based on the determined binding mode, we would like to know whether the docked structures are consistent with the aforementioned 3D-QSAR contour maps and can be used to qualitatively explain the experimental activity of the compounds.

Figure 3 shows the docked structure of the most active compound (**30**) binding with mPGES-1; some other representative binding structures are provided in the Supporting Information. The images of the docked structures were created by using Pymol.[28] The docking study reveals that the carboxyl group has a close electrostatic interaction with the Arg110 side chain. This explains the lower activity of compounds **6** and **7** in which the carboxyl group is replaced by an ester or amide group. The biphenyl group substituted

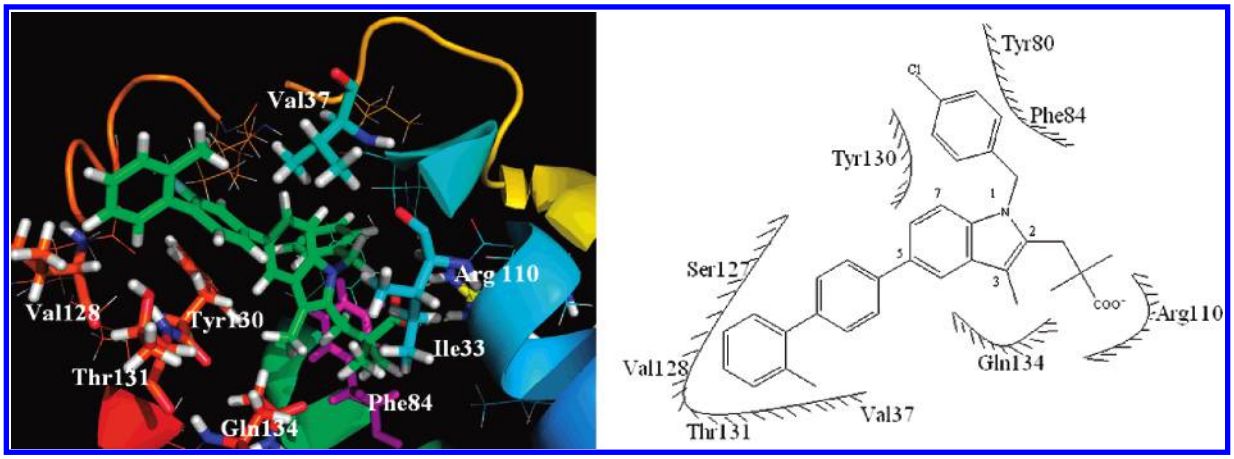

Figure 3. Structure of compound **30** binding with mPGES-1. The figure on the left side is the docked structure, and the figure on the right side is a 2D representation of compound **30** in the active site of mPGES-1. The important residues are highlighted.

at position #5 of the indole ring interacts with hydrophobic residues Val37 and Val128. The 4-Cl-benzyl group substituted at position #1 of the indole ring has a hydrophobic interaction with Phe84 on one side and the phenyl ring of Tyr130 is present on the other side. The methyl group substituted at position #3 of the indole ring is present in close proximity to the Gln134 residue. This explains the lower activity of compounds with bulky substituents at this position as it has the steric clash with this residue. Comparing compound **14** with compound **1**, we find that the presence of the methyl group at this position is more favored than the bulky group. The experimental substituent effects on the activity agree well with the docking structures.

The docking study can also explain the increased activity of compound **10**. The -CH_2- group in position #3 of the indole ring orients the bulky group such that it has a favorable interaction with the surrounding hydrophobic residues. The 4-(*tert*-butyl)benzyl group has a favorable hydrophobic interaction with residues Ile33 and Val37, which explains the higher activity of the compound. Thr131 and Ser127 are located in close proximity to the terminal phenyl ring such that the hydroxyl group of these residues can form a hydrogen bond with a suitable substituent on the phenyl ring. For example, compound **29** having a carbonyl group on the terminal phenyl ring has an IC_{50} of 6 nM. The docking results demonstrate that the carbonyl group indeed forms a hydrogen bond with the Ser127 hydroxyl group. In compounds **2** and **3**, the 4-Cl-benzyl group substituted at position #1 of the indole ring was replaced by -H and -CH_3, respectively, and they have a lower inhibitory activity. This is consistent with our docked structures showing that the favorable hydrophobic interaction with the benzyl group will be lost when the benzyl group is replaced by smaller groups. Thus, all results obtained from the molecular docking are qualitatively consistent with the experimental activity of this series of compounds, suggesting that the binding modes determined by the molecular docking are reasonable.

Comparison of the Docked Structures with the 3D-QSAR Contour Maps. The enzyme−inhibitor binding structures obtained from the molecular docking with the 3D structural model of mPGES-1 model are all qualitatively consistent with the aforementioned contour maps generated by the CoMFA and CoMSIA models. For example, the docked structures demonstrate that the terminal phenyl ring is surrounded by Val128, Val37, and Thr131 residues. Further bulky substituents on this phenyl group will result in a steric clash with the surrounding residues. This is consistent with the 3D-QSAR contour maps, in which the terminal phenyl ring is in a green region surrounded by a yellow region. Both the CoMFA and CoMSIA models show a red contour region around the terminal phenyl ring (Figure 2). As discussed above, the docked structures show that the hydroxyl groups of Thr131 and Ser127 side chains are in close proximity to the terminal phenyl ring and form hydrogen bonds with the electronegative groups. The agreement between the docked structures and the 3D-QSAR contour maps suggests that the binding mode obtained from the molecular docking is reasonable and that the developed 3D-QSAR models are reliable. All of the results obtained from the 3D-QSAR analysis and molecular docking are consistent with the experimental activity data, further supporting the developed 3D-QSAR models and the enzyme−inhibitor binding structures determined in this study.

For a final comparison, we also developed an additional set of 3D-QSAR models (denoted by CoMFA-3a and CoMSIA-3b) based on the structures of the inhibitors in the docked enzyme−inhibitor complexes. The CoMFA-3a model has a q^2 value of 0.77, an r^2 value of 0.98, and an SEE value of 0.201, whereas the CoMSIA-3b model has a q^2 value of 0.75, an r^2 value of 0.99, and an SEE value of 0.165. The contour plots from these models are all qualitatively consistent with the aforementioned 3D-QSAR contour plots. These results further confirm the consistency between the docked binding structures and 3D-QSAR contour plots. The satisfactory binding structures obtained from the molecular docking also strongly suggest that the computational 3D structural model of mPGES-1 used in the molecular docking is reasonable for studying how mPGES-1 binds with inhibitors and, therefore, for performing future rational design of novel mPGES-1 inhibitors.

CONCLUSION

The combined 3D-QSAR analysis and molecular docking using a computational 3D structural model of mPGES-1 provide valuable insights concerning how mPGES-1 binds with inhibitors. The 3D-QSAR analysis has led to the development of two satisfactory 3D-QSAR models, including the CoMFA model ($r^2 = 0.981$; $q^2 = 0.915$) and CoMSIA model ($r^2 = 0.964$; $q^2 = 0.904$), for predicting the biological

activity of new compounds. The high r^2 and q^2 values of the CoMFA and CoMSIA models suggest that mPGES-1 binds with all of the recently reported inhibitors in a similar binding mode. The contour maps generated from the developed CoMFA and CoMSIA models provide useful concepts about the types of the protein environment surrounding the inhibitors. Molecular docking using the computational 3D structural model of mPGES-1 provides the detailed structures of mPGES-1 binding with the inhibitors. The docked structures are all consistent with the 3D contour maps generated from the developed CoMFA and CoMSIA models, suggesting that the binding mode obtained from the molecular docking is reasonable and that the developed 3D-QSAR models are reliable. All of the results obtained from the 3D-QSAR analysis and molecular docking are consistent with the experimental activity data, further supporting the developed 3D-QSAR models and the enzyme−inhibitor binding structures determined in this study. The satisfactory binding structures obtained from the molecular docking also strongly suggest that the computational 3D structural model of mPGES-1 used in the molecular docking is reasonable for studying how mPGES-1 binds with its inhibitors and, therefore, for performing future rational design of novel mPGES-1 inhibitors.

ACKNOWLEDGMENT

The research was supported in part by the National Institutes of Health, the Kentucky Science & Engineering Foundation, and the Center for Computational Sciences (CCS) at the University of Kentucky.

Supporting Information Available: Some computational details and additional results including 5 figures and 6 tables. This material is available free of charge via the Internet at http://pubs.acs.org.

REFERENCES AND NOTES

(1) Sampey, A. V.; Monrad, S.; Crofford, L. J. Microsomal prostaglandin E synthase-1: the inducible synthase for prostaglandin E_2. *Arthritis Res. Ther.* **2005**, *7*, 114−117.

(2) Murakami, M.; Naraba, H.; Tanioka, T.; Semmyo, N.; Nakatani, Y.; Kojima, F.; Ikeda, T.; Fueki, M.; Ueno, A.; Og-ishi, S.; Kudo, I. Regulation of prostaglandin E_2 biosynthesis by inducible membrane associated prostaglandin E_2 synthase that acts in concert with cyclooxygenase-2. *J. Biol. Chem.* **2000**, *275*, 32783−32792.

(3) Camacho, M.; Gerboiles, E.; Escudero, J.-R.; Anton, R.; Garcia-Moll, X.; Vila, L. Microsomal prostaglandin E synthase-1, which is not coupled to a particular cyclooxygenase isoenzyme, is essential for prostaglandin E_2 biosynthesis in vascular smooth muscle cells. *J. Thromb. Haemostasis* **2007**, *5*, 1411−1419.

(4) Uematsu, S.; Matsumoto, M.; Takeda, K.; Akira, S. Lipopolysaccharide−dependent prostaglandin E_2 production is regulated by the glutathione-dependent prostaglandin E_2 synthase gene induced by Toll-like receptor 4/MyD88/NF-IL6 pathway. *J. Immunol.* **2002**, *168*, 5811−5816.

(5) Kaemi, D.; Murakami, M.; Nakatani, Y.; Ishikawa, Y.; Ishi, T.; Kudo, I. Potential role of microsomal prostaglandin E synthase-1 in tumorigenesis. *J. Biol. Chem.* **2003**, *278*, 19396−19405.

(6) Kaemi, D.; Yamakawa, K.; Takegoshi, Y.; Mikami-Nakanishi, M.; Nakatani, Y.; Oh-ishi, S.; Yasui, H.; Azuma, Y.; Hirasawa, N.; Ohuchi, K.; Kawaguchi, H.; Ishikawa, Y.; Ishii, T.; Uematsu, S.; Akira, S.; Murakami, M.; Kudo, I. Reduced pain hypersensitivity and inflammation in mice lacking microsomal prostaglandin E synthase-1. *J. Biol. Chem.* **2004**, *279*, 33684−33695.

(7) Ikeda-Matsuo, Y.; Ota, A.; Fukada, T.; Uematsu, S.; Akira, S.; Sasaki, Y. Microsomal prostaglandin E2 synthase-1 is a critical factor of stroke−reperfusion injury. *Proc. Natl. Acad. Sci. U.S.A.* **2006**, *103*, 11790−11795.

(8) Murakami, M.; Kudo, I. Recent advances in the molecular biology and physiology of the prostaglandin E2 biosynthetic pathway. *Prog. Lipid. Res.* **2004**, *43*, 3−35.

(9) Claveau, D.; Sirinyan, M.; Guay, J.; Gordon, R.; Chan, C.-C.; Bureau, Y.; Riendeau, D.; Mancini, J. A. Microsomal prostaglandin E2 synthase is a major terminal synthase that is selectively up-regulated during cyclooxygenase-2 dependent prostaglandin E2 production in the rat adjuvant-induced arthritis model. *J. Immunol.* **2003**, *170*, 4738−4744.

(10) Oshima, H.; Oshima, M.; Inaba, K.; Taketo, M. M. Hyperplastic gastric tumors induced by activated macrophages in COX-2/mPGES-1 transgenic mice. *EMBO J.* **2004**, *23*, 1669−1678.

(11) Engblom, D.; Saha, S.; Engstrom, L.; Westman, M.; Audoly, L. P.; Jakobsson, P. J.; Blomqvist, A. Microsomal prostaglandin E synthase-1 is the central switch during immune-induced pyresis. *Nat. Neurosci.* **2003**, *6*, 1137−1138.

(12) Simmons, D. L.; Botting, R. M.; Hla, T. Cyclooxygenase isozymes: The biology of prostaglandin synthesis and inhibition. *Pharmacol. Rev.* **2004**, *56*, 387−437.

(13) Silverstein, F. E.; Faich, G.; Goldstein, J. L.; Simon, L. S.; Pincus, T.; Whelton, A.; Makuch, R.; Eisen, G.; Agrawal, N. M.; Stenson, W. F.; Burr, A. M.; Zhao, W. W.; Kent, J. D.; Lefkowith, J. B.; Verburg, K. M.; Geis, G. S. Gastrointestinal toxicity with celecoxib vs nonsteroidal anti-inflammatory drugs for osteoarthritis and rheumatoid arthritis. The CLASS study: A randomized controlled trial. *JAMA* **2000**, *284*, 1247−1255.

(14) Caldwell, B.; Aldington, S.; Weatherall, M.; Shirtcliffe, P.; Beasley, R. Risk of cardiovascular events and celecoxib: a systematic review and meta-analysis. *J. R. Soc. Med.* **2006**, *99*, 132−140.

(15) Dickman, A.; Ellershaw, J. NSAIDS: gastroprotection or selective COX-2 inhibitor? *Palliative Med.* **2004**, *18*, 275−286.

(16) Grosser, T.; Fries, S.; FitzGerald, G. A. Biological basis of the cardiovascular consequences of COX-2 inhibition: therapeuticchallenges and opportunities. *J. Clin. Invest.* **2006**, *116*, 4−15.

(17) Cheng, Y.; Wang, M.; Yu, Y.; Lawson, J.; Funk, C. D.; FitzGerald, G. A. Cyclooxygenases, microsomal prostaglandin E synthase-1, and cardiovascular function. *J. Clin. Invest.* **2006**, *116*, 1391−1399.

(18) Mehrotra, S.; Morimiya, A.; Agarwal, B.; Konger, R.; Badve, S. Microsomal prostaglandin E2 synthase-1 in breast cancer: a potential target for therapy. *J. Pathol.* **2006**, *208*, 356−363.

(19) Riendeau, D.; Aspiotis, R.; Ethier, D.; Gareau, Y.; Grimm, E. L.; Guay, J.; Gurial, S.; Juteau, H.; Mancini, J. A.; Methot, N.; Rubin, J.; Friesen, R. W. Inhibitors of the inducible microsomal prostaglandin E2 synthase (mPGES-1) derived from MK-886. *Bioorg. Med. Chem. Lett.* **2005**, *15*, 3352−3355.

(20) Huang, X.; Yan, W.; Gao, D.; Tong, M.; Tai, H.-H.; Zhan, C.-G. Structural and functional characterization of human microsomal prostaglandin E synthase-1 by computational modeling and site directed mutagenesis. *Bioorg. Med. Chem.* **2006**, *14*, 3553−3562.

(21) Butterfoss, G. L.; Kuhlman, B. Computer-based design of novel protein structures. *Ann. Rev. Biophys. Biomol. Struct.* **2006**, *35*, 49−65.

(22) Juan, A. A. S.; Cho, S. J. 3D-QSAR study of microsomal prostaglandin E_2 synthase (mPGES-1) inhibitors. *J. Mol. Model.* **2007**, *13*, 601−610.

(23) Cramer, R. D.; Patterson, D. E.; Bunce, J. D. Comparative molecular field analysis (CoMFA). 1. Effect of shape on binding of steroids to carrier proteins. *J. Am. Chem. Soc.* **1988**, *110*, 5959−5967.

(24) Debnath, A. K. Quantitative structure-activity relationship (QSAR) paradigm −Hansch era to new millennium. *Mini Rev. Med. Chem.* **2001**, *1*, 187−195.

(25) Frisch, M. J.; Trucks, G. W.; Schlegel, H. B.; Scuseria, G. E.; Robb, M. A.; Cheeseman, J. R.; Montgomery, J. A., Jr.; Verven, T.; Kudin, K. N.; Burant, J. C.; Millam, J. M.; Iyengar, S. S.; Tomasi, J.; Barone, V.; Mennucci, B.; Cossi, M.; Scalmani, G.; Rega, N.; Petersson, G. A.; Nakatsuji, H.; Hada, M.; Ehara, M.; Toyota,K.; Fukuda, R.; Hasegawa, J.; Ishida, M.; Nakajima, T.; Honda, Y.; Kitao, O.; Nakai, H.; Klene, M.; Li, X.; Knox, J. E.; Hratchian, H. P.; Cross, J. B.; Adamo, C.; Jaramillo, J.; Gomperts, R.; Stratmann, R. E.; Yazyev, O.; Austin, A. J.; Cammi, R.; Pomelli, C.; Ochterski, J. W.; Ayala, P. Y.; Morokumo, K.; Voth, G. A.; Salvador, P.; Dannenberg, J. J.; Zakrzewski, V. G.; Dapprich, S.; Daniels, A. D.; Strain, M. C.; Farkas, O.; Malick, D. K.; Rabuck, A. D.; Raghavachari, K.; Foresman, J. B.; Ortiz, J. V.; Cui, Q.; Baboul, A. G.; Clifford, S.; Cioslowski, J.; Stefanov, B. B.; Liu, G.; Liashenko, A.; Piskorz, P.; Komaromi, I.; Martin, R. L.; Fox, D. J.; Keith, T.; Al-Laham, M. A.; Peng, C. Y.; Nanayakkara, A.; Challacombe, M.; Gill, P. M.; Wong, M. W.;

Gonzalez, C.; Pople, J. A. *Gaussian 03, Revision A.1*; Gaussian: Pittsburgh, PA, 2003.
(26) Rarey, M.; Kramer, B.; Lengauer, T.; Kleb, G. A fast flexible docking method using an incremental construction algorithm. *J. Mol. Biol.* **1996**, *261*, 470−489.
(27) Olofsson, K.; Suna, E.; Pelchman, B.; Ozola, V.; Katkevics, M.; Kalvins, I.; Schaal, W. Preparation of indolecarboxylates as inhibitors of microsomal prostaglandin E synthase-1 (mPGES-1) useful in the treatment of inflammation. PCT Intl. Appl. WO 2005/123675, December 29, 2005.
(28) Delano, W. L. *The Pymol Molecular Graphics System*; Delano Scientific: Palo Alto, CA, 2002.

CI700315C